agronomy

MDPI

Article

Biodegradable Carboxymethyl Chitosan/Polyvinyl Alcohol Hymexazol-Loaded Mulch Film for Soybean Root Rot Control

Ze Lv, Xiaohan Meng, Shaoyang Sun, Tianzhen Jiang, Shengfu Zhang and Jianguo Feng *

College of Plant Protection, Yangzhou University, Yangzhou 225009, China
* Correspondence: jgfeng@yzu.edu.cn; Tel.: +86-0514-87979395

Abstract: Soybean root rot is an important disease that has affected soybean crops in recent years, but the available control methods still do not provide good protection for soybeans. In this study, three biodegradable mulch films (HML@CMCS, HML@PVA, HML@CMCS/PVA) were prepared from carboxymethyl chitosan (CMCS) and polyvinyl alcohol (PVA), and hymexazol (HML) was loaded on them. The surface and cryofractured surface were compared via micromorphological observations using SEM, AFM, and 3D measurements. Mechanical, water barrier, and optical properties were compared between the different films, and the results showed that the composite film (HML@CMCS/PVA) had better tensile properties, lower water content (35%), and lower water solubility (28%), while water barrier properties were significantly improved. HML@CMCS/PVA also had better light transmission than commercial films (opacity at 600 nm of 1.92). Finally, the composite film was selected to study antifungal properties, soil degradability, and biosafety. The results showed that it exhibited significant inhibitory activity against *Fusarium oxysporum* and could effectively control soybean root rot, while degradation reached 58% after 7 d of soil burial, and the mortality of earthworms relative to the microplastics produced by the film within 7 d (23.33%) was much lower than that of the commercial film, demonstrating its excellent biosafety. This study provides a new approach for the on-farm management of soybean root rot and the reduction in soil microplastic pollution.

Keywords: carboxymethyl chitosan; polyvinyl alcohol; hymexazol; biodegradable film; *Fusarium oxysporum*

Citation: Lv, Z.; Meng, X.; Sun, S.; Jiang, T.; Zhang, S.; Feng, J. Biodegradable Carboxymethyl Chitosan/Polyvinyl Alcohol Hymexazol-Loaded Mulch Film for Soybean Root Rot Control. *Agronomy* **2023**, *13*, 2205. https://doi.org/10.3390/agronomy13092205

Academic Editor: Robert P. Larkin

Received: 21 July 2023
Revised: 19 August 2023
Accepted: 22 August 2023
Published: 24 August 2023

1. Introduction

Soybean (*Glycine max* L. Merr.) is a highly valued cash crop due to its abundant vegetable proteins and oils. Nevertheless, pests, weeds, and diseases pose significant threats to soybean production. Among these, soybean root rot (SRR) caused by *Fusarium oxysporum* (*F. oxysporum*) is particularly detrimental and results in substantial yield losses [1–3]. SRR stands out as the most threatening disease transmitted through soil, which inflicts pod blight, seed decay, wilt, and crown root decay in temperate regions [4]. It has been shown that soil conditions such as temperature and humidity are the main affected factors due to infection [5]. Hence, regulating soil temperature and humidity by mulching is a very effective way to control SRR.

Plastic films are widely used in soybean growing seasons because of their excellent soil water retention and insulation capabilities [6,7]. However, there have been numerous reports of plastic films that are not recycled at harvest, resulting in large amounts of plastic debris being incorporated into farm fields and remaining in the soil environment for decades or longer, which seriously affects soil quality and crop yield [8,9]. Therefore, there is a need to develop a biodegradable film in order to mitigate agro-ecological stress while controlling SRR.

Currently, materials made from various biodegradable polymers are widely used in agricultural production and food freshening [10,11]. Natural polymers have received a lot

of attention due to their renewable, abundant, and inexpensive nature, while factors such as the movement of natural polymers in the film matrix and the interactions between polymer functional groups favor the construction of films with excellent barrier properties [12,13]. Chitosan has demonstrated antiviral, antibacterial, and antifungal properties, which have been explored for many agricultural uses. Furthermore, it has become a well-established film-forming material, but insolubility is the main problem affecting its application [14,15]. CMCS is an amphoteric derivative of chitosan prepared by introducing carboxymethyl groups into the amino, primary, and secondary hydroxyl sites of the glucosamine moiety [16]. CMCS retains several properties of chitosan, including its good film-forming properties, making it an attractive biofilm material [17]. However, high-water solubility is also an indicator of a lower water barrier, which may limit the broad application of used CMCS [18]. In biofilm development, PVA is used because of its good film-forming ability, complete biodegradability, crystal modulus, and wide range of crystallinity, but its inherent brittleness and rigidity leads to the necessity of blending it with other materials in order to prepare film materials with excellent properties [19–21]. Therefore, replacing commercial plastic film with biodegradable plastic film can not only effectively control soybean SRR, but also meet the innovative needs of sustainable agricultural development.

In this study, the main objective was to propose a new bio-safety film that can effectively control SRR in soybean while reducing the environmental stress caused by the film. We hypothesized that mixing CMCS with PVA to prepare HML-loaded films could improve the mechanical and barrier properties of the films, as well as effectively inhibit SRR. In the course of the study, the macroscopic morphology of the films was compared and their microscopic morphology was observed using scanning electron microscopy (SEM), atomic force microscopy (AFM), and three-dimensional (3-D) measuring instruments. The excellent performance of the composite films was verified by comparing the tensile, water barrier, and optical properties. Finally, the antifungal activity, soil degradability, and soil biosafety of the composite films were also studied over a period of 7 d. This study provides a biodegradable bio-based film with efficient antifungal properties, which will provide a new approach to control SRR effectively and reduce agricultural microplastic pollution.

2. Materials and Method

2.1. Materials

Hymexazol (95.0%) was purchased from Shanxi Qixing Pesticide Co., Ltd. (Yuncheng, China). Carboxymethyl chitosan (Mw = 400 kDa, Substitution degree of carboxymethyl $\geq$ 80%) was purchased from Shanghai Yuanye Biochemical Technology Co., Ltd. (Shanghai, China), and polyvinyl alcohol was provided by Shanghai Aladdin Biochemical Technology Co., Ltd. (Shanghai, China). Glycerol was provided by Sinopharm Chemical Reagent Co., Ltd. (Shanghai, China). *F. oxysporum* (1-F5, internal fungal collection) was collected in 2022 from soybean plants in Heilongjiang Province, China.

2.2. Preparation of Films

The films were prepared using the solution casting method [22]. CMCS and PVA were mixed in a ratio (0:2, 1:1, 2:0) and added to the HML aqueous solution containing 7 mg, deionized water was added until it reached 100 mL, and 0.7 g of glycerol was added dropwise. The resulting liquid was heated at 95 °C for 3 h. The prepared film solution was cast in a petri dish (10 cm × 10 cm), dried at 40 °C for 12 h, and then dried at room temperature to a constant weight. The obtained samples were defined as HML@PVA, HML@CMCS, and HML@CMCS/PVA, respectively.

2.3. Characterization

2.3.1. SEM

The surface and cryofractured surface structure of HML@CMCS, HML@PVA, and HML@CMCS/PVA was examined and observed after drying for 48 h using a Gemini SEM 300 (Carl Zeiss, Jena, Germany). The specimens were prepared and quenched using the

liquid nitrogen immersion method, and the films were fixed to the specimen holder with gold-coated double-sided adhesive tape. The cryofractured surfaces were then examined at an accelerating voltage of 2 kV [23].

2.3.2. Three-Dimensional Measurements

An LSM 700 (Carl Zeiss, Jena, Germany) was used to observe the cryofractured surface and to measure the film thickness of the film samples treated with the liquid nitrogen impregnation method. The measured results were compared with micrometer measurements [24]. The average values were used to determine opacity, water vapor permeability (WVP), and mechanical properties.

2.3.3. AFM

The surface of the film was analyzed using AFM to compare the change in the surface roughness of the sample. Three statistical parameters related to the sample's roughness were calculated for the 3 µm × 3 µm scanning area: the average roughness (R_a: mean of the absolute value of the mean surface height's deviation), the root mean square roughness (R_q: mean of the root mean square of the mean data plane height's deviation), and the maximum value in z-direction (R_z) [25].

2.3.4. Mechanical Properties

The mechanical properties of the experimental film materials were determined. The films were cut into strips (10 mm × 60 mm) and placed at 25 °C for 48 h. The test method was in accordance with the national standard GB/T 1040.1-2018 [26]. The tests were carried out at 25 °C and 5.00 mm min^{-1} using an experimental speed tester (Zhiqu, ZQ-990LB, Dongguan, China). HML@CMCS, HML@PVA and HML@CMCS/PVA were analyzed by stress-strain curves, Young's modulus (YM), tensile strength (TS), and elongation at break (EAB). The experiment was repeated three times for each sample. YM was calculated using Equation (1):

$$Young's\ modulus = \frac{FL_0}{A\Delta L} \quad (1)$$

where A denotes the cross-sectional area (m^2), L_0 denotes the initial length of the film (m), F denotes the tensile force in Newtons (N), and ΔL denotes the change in length after stretching (m).

2.3.5. Water Barrier Properties: WC, WS, WVP

The *WC* of each pretreated film was determined in triplicate by drying the sample (20 × 20 mm) at approximately 105 °C for 24 h. *WC* was expressed as a percentage of the total weight. *WC* was calculated using Equation (2):

$$WC = \frac{m_1 - m_0}{m_0} \times 100\% \quad (2)$$

where m_0 and m_1 denote the masses of the film before and after drying, respectively.

WS tests were performed by placing the completely dried film samples (20 × 20 mm) in a 50 mL glass container at room temperature for 24 h. After removing excess water, the remaining undissolved films were recovered and dried at 105 °C for 24 h. *WS* was calculated using Equation (3):

$$WS = \frac{m_1 - m_2}{m_1} \times 100\% \quad (3)$$

where m_2 denotes the remaining mass after dissolution.

The measurement of the water vapor permeability (WVP) of the film was carried out using the appropriately adapted ASTM E-96 standard method (ASTM, 1990) [27]. The sample cups were filled with 5 g of $CaCl_2$, and the film samples were set at the mouth of the cups and sealed with rubber seals. The cups were left at room temperature (temperature:

23 ± 2 °C; relative humidity (RH): 50 ± 5%). The change in the weight of the sample cup was calculated every 24 h. The *WVP* was calculated as follows:

$$WVP = \frac{\Delta m}{\Delta t} \frac{x}{S\Delta P} \quad (4)$$

where Δm indicates the difference in mass before and after, Δt indicates the difference in measurement time, x represents the film thickness, S represents the surface area of the film that is in contact with the bottle mouth, and ΔP represents the partial pressure difference in the film.

2.3.6. Optional Properties: Transmittance and Transparency Properties and Color

The films were cut to a size of 50 mm × 50 mm and the transmittance of the films was measured in the wavelength range of 200–800 nm using a UV-visible-NIR absorption spectrometer (Cary 5000 Varian, Palo Alto, CA, USA); in addition, five measurements were taken for each of the two products prepared. The transparency value (T) at 600 nm was calculated according to Equation (5):

$$T = \frac{-logT_{600}}{x} \quad (5)$$

where T_{600} denotes the percentage of transmittance at 600 nm, and x denotes the film's thickness (mm). A high T value shows low film transparency.

The color of the films was measured using a colorimeter (CS-420, Hangzhou, China). Films with a diameter of 10 mm were laid flat on a standard white mirror plate using a CIELAB-grade measurement color as the base color. L^* (brightness), a^* (redness/greenness), and b^* (yellowness/blueness) values were recorded. Five replicates were performed for each sample. The total color difference (ΔE) was calculated using Equation (6):

$$\Delta E = \sqrt{(L - L^*)^2 + (a - a^*)^2 + (b - b^*)^2} \quad (6)$$

where L, a, and b denote the color indices of the standard white plate.

2.3.7. XRD

The film is cut to a size of 50 × 50 mm and the X-ray diffraction patterns of the films were measured using an X-ray diffractometer fitted with Cu Ka (D8 Focus Bruker, Karlsruhe, Germany) at 40 kV and 40 mA over a range from 5° to 80°.

2.3.8. FT-IR

FT-IR analysis of thin films was performed using a TENSOR27 FTIR spectrometer (BRUKER, Karlsruhe, Germany) equipped with gemstone accessories within the range of 4000 to 400 cm^{-1} with a nominal resolution of 4 cm^{-1}, and HML was analyzed using FT-IR at the same range with a resolution corresponding to the KBr press method.

2.4. In Vitro Antifungal Properties

The in vitro antifungal assay was performed in reference to Liang et al. [23]. *F. oxysporum* was cultured on potato agar plates (90 mm) and placed at 28 °C in the dark. After a period of time, it was used as a fungal source in membranes for an in vitro activity assay. The prepared CMCS/PVA, HML@CMCS/PVA and sterile filter paper of the same size (UV sterilized for 20 min) were placed symmetrically on potato agar plates with mycelium plates of the same size, and incubated at 28 °C in a dark environment to evaluate their in vitro inhibitory activities within 7 d. The sterile filter paper treatment and CMCS/PVA treatment were used as control groups, and three replicates were set up for each group of experiments.

2.5. Biosafety of Films to Earthworms

The method of the earthworm purging experiment was based on the method of Ding et al. [28] and adjusted appropriately. The body surface of each earthworm was

washed with deionized water and placed individually in a Petri dish containing 5 mL of deionized water with five 2 mm diameter holes drilled in the lid to allow air to enter; the earthworms were then starved in the dark at 16 °C for 2 d. After washing again, 10 earthworms were placed in 500 g of soil as a reserve. Commercial film, CMCS/PVA, and HML@CMCS/PVA were ground at 0.01, 0.1, and 0.5% respectively and added to the soil as food for the earthworms and the mortality rate of the earthworms was observed for 7 consecutive days.

2.6. Soil Degradation Experiments

The soil burial experiments were carried out according to the method of Mantia et al. [29] with appropriate modifications. The soil (loam soil) was collected from an experimental field from Yangzhou University with a depth of 0~15 cm. Soil samples were taken from 14 jars of the same size and weight as the jars used for HML@PLA/CMCS (0.342 g) or commercial films (0.124 g), and they were buried 10 cm deep in each jar. The treated soil samples were tested at a constant humidity in a room temperature environment, and the degradation of the films was observed from 1 to 7 d; the degradation rate was calculated using Equation (7):

$$Degradation\ rate = \frac{m_3 - m_4}{m_3} \times 100\% \quad (7)$$

where m_3 and m_4 are the initial weight of the film and the mass of the remaining film after the soil degradation treatment, respectively.

2.7. Statistical Analysis

The results of the experiments were presented as the mean value accompanied by the standard deviation (SD). The statistical analysis of the data was conducted via the utilization of SPSS ANOVA Statistics 26 software, specifically IBM version 21.

3. Result and Discussion

3.1. Morphologies of Films

Microstructural observations were carried out on the surface and cryofractured surface of the films, as shown by SEM imaging (Figure 1A). The microstructural results were not significantly different from macroscopic observations. As clearly observed by SEM images, HML@CMCS exhibits a rough and inhomogeneous surface. The surface structure of HML@PVA is uniform and dense, flat and smooth, with no surface defects or holes, while the cryofractured surface of HML@PVA is slightly inhomogeneous, exhibiting many fine pores with banded stripes. After blending, the surface and cross-section of HML@CMCS/PVA were smooth and continuous, indicating a compact polymer chain arrangement. With the addition of CMCS, the observed porosity and roughness of the network structure of HML@CMCS/PVA increased. The reason for this phenomenon is the strong bonding interaction between the hydroxyl group of the PVA molecule and the carboxymethyl group of the CMCS molecule, indicating higher compatibility and blend homogeneity between the two polymers. This results in HML@CMCS/PVA with a homogeneous top layer and a smooth cryofractured surface [30,31].

Figure 1B shows the surface morphology of the three films obtained using AFM scanning, and the roughness parameters obtained from the analysis are shown in Table 1. They are more realistic for determining the surface roughness of films. The brightest regions represent the highest points or nodules, and the darker regions constitute valleys or film pores. In agreement with SEM results, the surface of HML@CMCS has a porous and uneven structure with the highest roughness coefficient; moreover, with the addition of PVA, the surface is homogeneous and smooth, and its roughness decreases significantly, showing the high compatibility between CMCS and PVA and the homogeneous surface of the resulting film [32]. The reduction in surface roughness led to a decrease in the average pore size, which was confirmed via SEM analysis [33]. In addition, the reduced surface roughness is a favorable factor in reducing the fouling of the composite film.

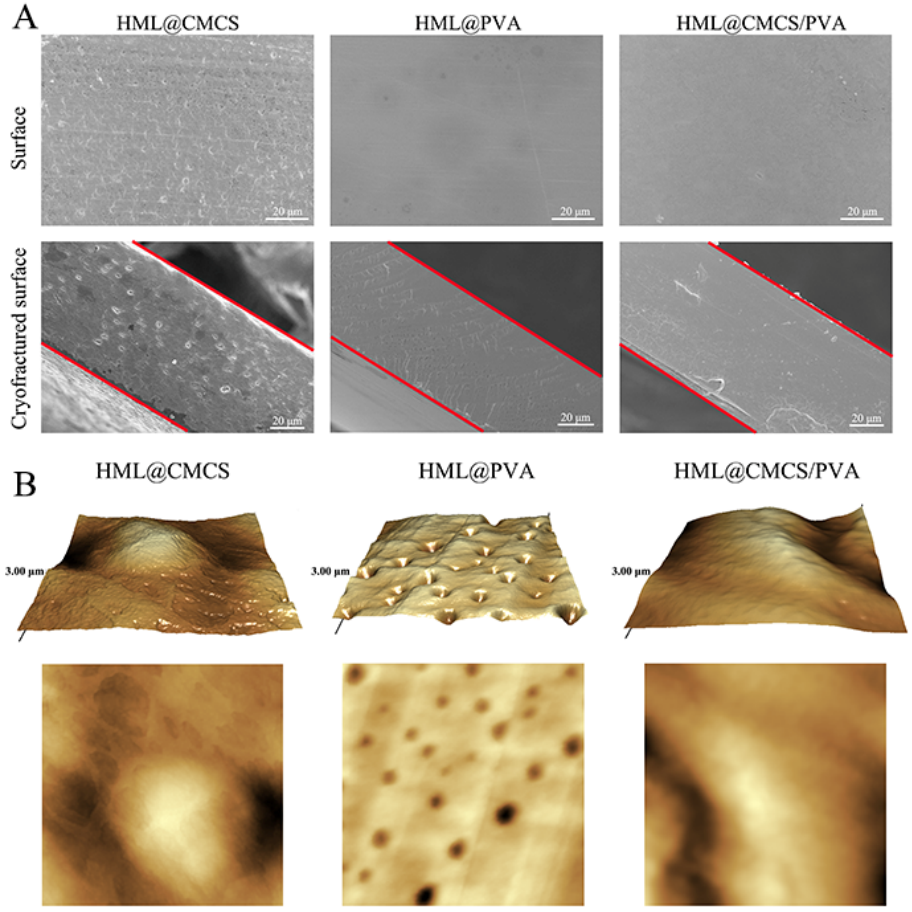

Figure 1. (**A**) SEM images of the films' surface and cryofractured surface. (**B**) AFM images of the films surface.

Table 1. Surface roughness coefficients of different film samples.

Film	R_a	R_z	R_q
HML@CMCS	51.804	258.990	61.648
HML@PVA	2.779	31.476	3.779
HML@CMCS/PVA	13.765	89.177	17.17

The cryofractured surfaces of the three film samples were observed using 3D scanning, and their cryofractured surface widths were measured; the measured results were the film's thicknesses. The results show that the cross sections of the three film samples observed in 3D scanning are consistent with the SEM results, as shown in Figure 2A. The measured film thicknesses are shown in Figure 2B, and the thicknesses of HML@CMCS, HML@PVA, and HML@CMCS/PVA are 101.72 μm, 56.68 μm, and 85.92 μm, respectively. The section's widths observed using 3D laser microscopy measurements were not significantly different from micrometer measurements (Figure 2C).

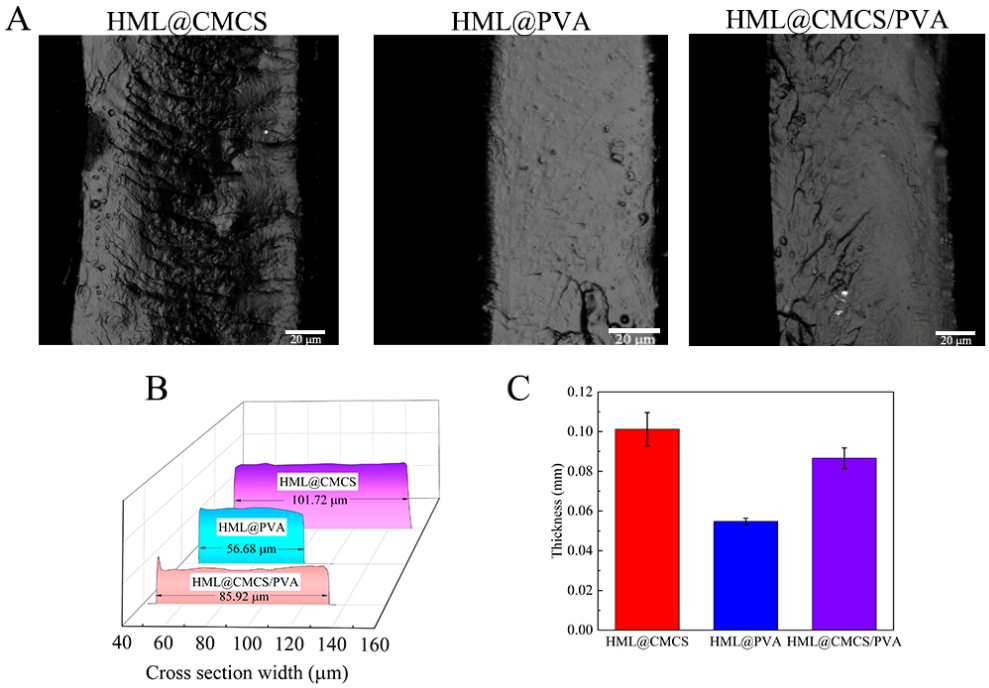

Figure 2. A 3-D scanned image (**A**) of the films cryofractured surface and the thickness obtained by 3-D scanning (**B**). Thickness (**C**) of the film samples measured by a micrometer.

3.2. Mechanical Properties of Films

Excellent mechanical properties of the film are necessary for long term use in agricultural fields. Therefore, four classic properties of HML@CMCS, HML@PVA, HML@CMCS/PVA were investigated: stress-strain curve, TS, EAB, and YM. Figure 3A shows the stress variation with the strain for the three film samples. The mechanical properties of pure HML@PVA films are influenced by the degree of hydrolysis and molecular weight. Due to the inherent brittleness and rigidity of PVA, its blending with CMCS significantly improves the tensile properties of HML@CMCS/PVA [26]. Figure 3B shows the TS of the three films. It can be clearly observed that with the addition of PVA, the TS of the blended film reaches 13.7 MPa. Figure 3C shows the EAB of the films. The EAB of HML@CMCS/PVA is reduced to 124.7% after blending the two materials, as the increase in TS for thin film materials often comes at the cost of a lower EAB. Intermolecular hydrogen bonding restricts the movement of molecular chain segments, leading to a decrease in EAB. The YM of the three film materials is shown in Figure 3D. The YM of HML@CMCS/PVA-blended films is significantly higher compared to pure films, which is attributed to the combination of intermolecular forces, water content, material compatibility, the properties of the blended polymers, and the processing conditions that determine the mechanical properties of HML@CMCS/PVA-blended films [34,35]. The increase in YM implies the incorporation of CMCS, which provides the blended films with better deformation resistance compared to HML@PVA [36]. Compared to HML@CMCS and HML@PVA, the improved mechanical properties of HML@CMCS/PVA prove its excellent application in agriculture.

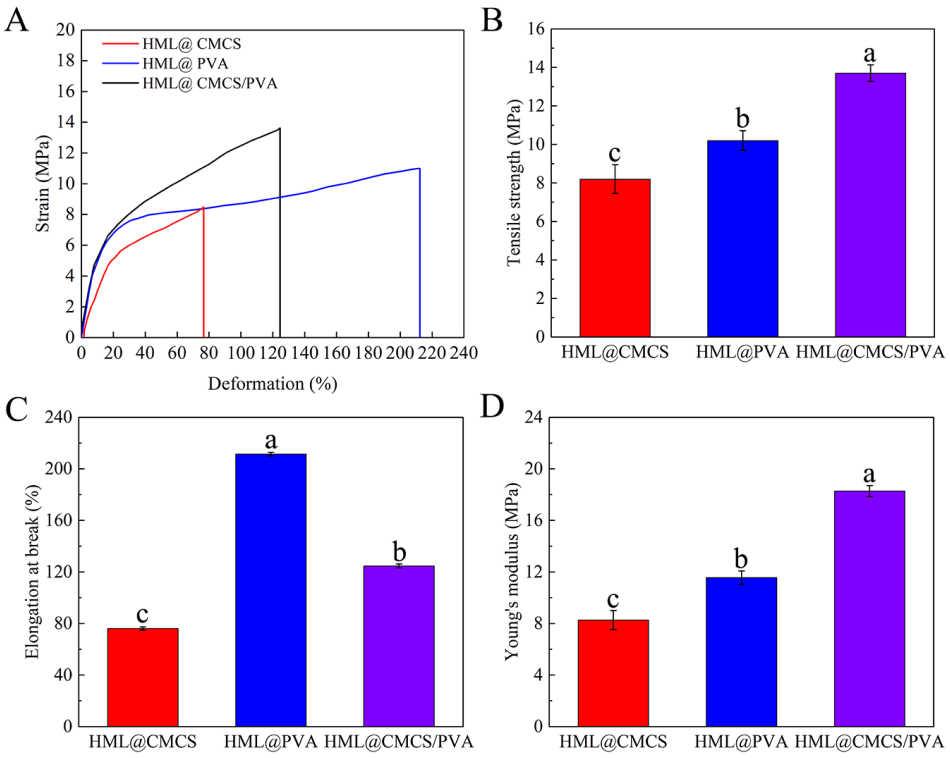

Figure 3. Stress–strain curves (**A**), tensile strength (**B**), elongation at break (**C**), and Young's modulus (**D**) images of different film samples. Different letters for the same test parameter indicate significant differences among different groups ($p < 0.05$).

3.3. Water Barrier Properties of Films

The water retention and self-cleaning ability of the film is a concern for practical applications on agriculture [37]. The insolubility or water barrier of the film is an important feature, as it inevitably needs to be in contact with water when used for soil cover. To illustrate the changes in hydrophilicity on the film surface, the WC (Figure 4A) and WS (Figure 4B) of HML@CMCS, HML@PVA, and HML@CMCS/PVA were compared. The WC and WS of HML@CMCS reached 9% and 9.5%, respectively, the WC and WS of HML@PVA reached 11% and 35%, respectively, while the WC (35%) and WS (28%) of HML@CMCS/PVA increased. This may be because the bonding strength between CMCS and PVA is stronger than the hydrogen bond between molecules and water [38,39].

The conservation of water in the soil is an important reason for the use of mulch; thus, WVP is one of the most important reference factors for evaluating the performance of biodegradable mulch in practical applications [40,41]. Therefore, it is important to evaluate the WVP of the films. As shown in Table 2, the water vapor transmission rate (WVP) of HML@PVA was 0.8380 g mm/h m^2 kPa, whereas the blending of CMCS effectively solved the defect of the high WVP of HML@PVA, and the WVP of HML@CMCS/PVA was reduced to 0.7716 mm/h m^2 kPa. This may be due to the chemical bonding between CMCS and PVA, resulting in the formation of network structures in the film and the extension of the path length of water molecules through the material, thus improving the water repellency of the film [42]. The lower WVP ensures the availability of water required for the growth of soybean seedlings and prevents drought stress from harming the seedlings [43].

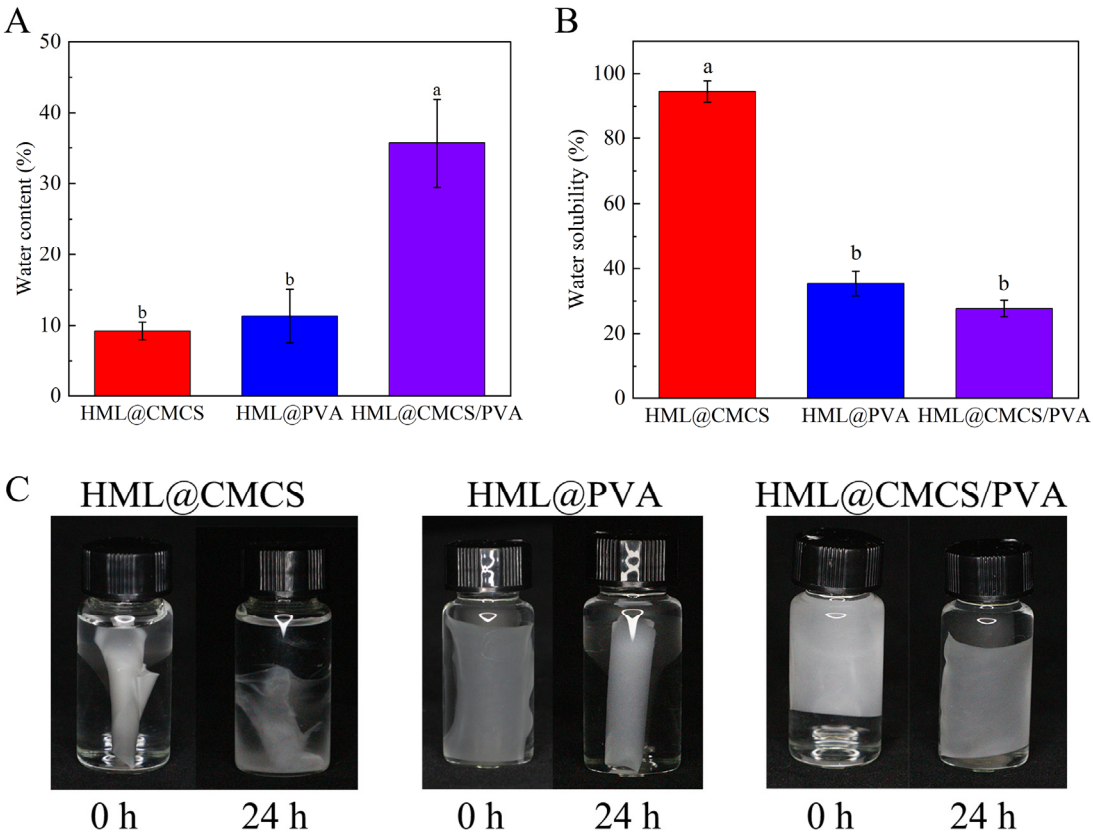

Figure 4. Water content (**A**), water solubility (**B**) and changes in water solubility after 24 h (**C**) of different film samples. Different letters for the same test parameter indicate significant differences among different groups ($p < 0.05$).

Table 2. Differences in the mean WVP values of different film samples over 7 d and the chromaticity coefficients of the film samples. Different letters for the same test parameter indicate significant differences among different groups ($p < 0.05$).

Film	WVP (g mm/h m^2 kPa)	L*	a*	b*	Δ*E*
HML@CMCS	0.4852	88.392 (0.092) ^{c}	−1.972 (0.010) ^{c}	5.584 (0.226) ^{a}	10.234 (0.242) ^{b}
HML@PVA	0.8380	91.754 (0.062) ^{a}	−1.246 (0.015) ^{a}	−3.956 (0.042) ^{c}	0.158 (0.045) ^{c}
HML@CMCS/PVA	0.7716	89.903 (0.032) ^{b}	−1.363 (0.029) ^{b}	−0.157 (0.159) ^{b}	18.783 (1.357) ^{a}

By observing the solubility (Figure 4C) of CMCS/PVA in water after HML loading, it was evident that HML@CMCS/PVA was relatively weakly soluble. When observed using immersion in deionized water, CMCS/PVA exhibited a distinct curl immediately after contact with water, whereas HML@CMCS/PVA had a flattened shape due to the reduced hydrophilicity caused by hydrogen bonding between the molecules. After 24 h of immersion, both films maintained their integrity (Figure 2D). The mixing of different polymer molecules slows down the decomposition of the film in water, prolonging the life of water-soluble films.

3.4. Optical Properties of Films

Different color films have different light transmissions, which affect their light insulation capacity [44]. The L* value reflects the surface brightness of the film, and the value varies from 0 (black) to 100 (white). The a* color difference value represents redness and greenness, with a larger a* representing greater redness. The b* value represents yellowness

and blueness, with a larger b* representing greater yellowness. The total color difference (ΔE) serves as an indicator for the comprehensive evaluation of films. As observed in Table 2, after blending the two polymers, the L*, a*, and b* of the prepared films are higher than that of HML@CMCS and lower than that of HML@PVA, which ultimately leads to an increase in ΔE. This may be due to the cross-linking effect between the different polymers that affect the color difference of the blended films. It reflects the modulating effect of PVA on the chromaticity of pure CMCS films. However, numerically, the main difference between the three film samples is reflected in their yellowish blueness, which is attributed to the yellow color of CMCS itself, leading to a larger b* value of the resulting film [45,46], which is well ameliorated by the addition of PVA.

Films are widely used in agriculture due to their good insulating properties, and different transmittances determine different solar energy absorption capacities [47]. We compared the abilities of HML@CMCS, HML@/PVA, HML@CMCS/PVA, and commercial film to transmit UV light (Figure 5A). It was reported that only 6.8% of the energy of solar light is distributed below 400 nm, and 54.3% of the energy distribution is within the range of 760–3000 nm [48,49]. The transmittance of HML@CMCS/PVA was significantly higher than that of HML@CMCS after 400 nm due to the difference in film thickness and polymer crystallinity, confirming that the incorporation of PVA improved the transmittance of CMCS, and this is numerically much lower than commercial films. Meanwhile, within the range of 200–400 nm, the shielding ability of HML@CMCS/PVA against UV light was significantly elevated due to CMCS, which helped mitigate its effect on the stability of pesticides in the films [50]. The opacities of HML@CMCS, HML@/PVA, and HML@CMCS/PVA were compared to those of commercial film at 600 nm in Figure 5B. The opacity of the prepared HML@CMCS/PVA (1.92) is much lower than that of the commercial film, which is due to the difference in thickness between the two films, and further indicates that the prepared composite film has good light transmission properties.

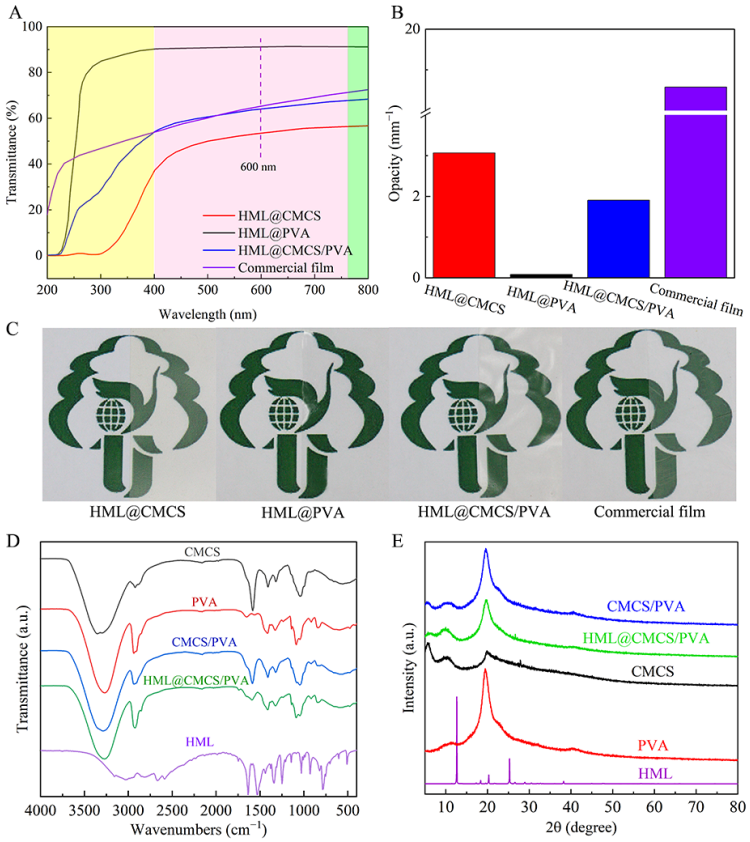

Figure 5. Transmittance for different wavelengths of light (**A**), opacity at 600 nm (**B**), the appearance (**C**), FT-IR scanning images (**D**), and XRD scanning images (**E**) of different film samples.

Observing the appearance of the film macroscopically, it can be clearly known that the prepared HML@CMCS is light yellow, and HML@PVA is highly transparent. After the two are mixed, the yellow color is obviously weakened, which is consistent with the chromaticity measurement results, but the difference between L* and a* is difficult to observe when performing visual inspections. At the same time, the transparency of HML@CMCS/PVA is significantly better than that of commercial film, which is also consistent with the test results of light transmittance and opacity.

3.5. FT-IR

For CMCS, peaks around 1585.2 and 1413 cm^{-1} corresponded to antisymmetric and symmetric stretching vibrations for the -COO- group, respectively [51]. With respect to the FTIR spectra of PVA, the absorption peak at 2936 cm^{-1} is responsible for the -CH_2 stretching vibration [52]. Absorption peaks due to -OH vibrations at 3324 cm^{-1}, absorption peaks due to C-H vibrations at 2941 and 1331 cm^{-1}, and -CH_2- vibrations at 1425 cm^{-1} were observed for the PVA chain structure [53]. The addition of CMCS to PVA shifted the -CH_2 stretching vibration to a lower wave number; these results indicate that PVA crosslinks well with CMCS. It was also observed in HML@CMCS/PVA that HML displayed a pair of intense absorption peaks at 1747 cm^{-1}, which was attributed to the acyl stretching vibration peaks due to acyl groups (C=O) on the oxazole ring, proving the successful loading of HML onto the CMCS/PVA film.

3.6. XRD

The presence of crystalline regions in the XRD patterns shows a lack of interaction between the surface's polymer components. Therefore, in a mechanical mixing environment, the X-ray diffraction pattern is expressed as a mixture of various components. The appearance of a sharp peak at $2\theta = 20^\circ$ in the XRD pattern of CMCS is attributed to the special crystalline nature of CMCS, which corresponds to crystalline type II [54]. The structure of PVA as a semi-crystalline polymer is confirmed by the presence of broad peaks within the 15–25° range in its XRD pattern. Also, there is an XRD peak centered on the orthorhombic lattice at 19.5°, which corresponds to an average molecular spacing of 4.57 Å and is assigned to the (101) plane. An additional peak at 40.5° was assigned to the (202) reflection [55]. After mixing, HML@CMCS/PVA exhibits a similar structure to PVA. The decrease in peak intensity at 19.5° is also attributed to the mixing of CMCS with PVA [56]. No formations of crystalline regions were observed in the HML@CMCS/PVA film due to the network structure formed by the groups (hydroxyl and carboxymethyl) between the two polymer molecules. This indicates a reduced extent of crystalline regions in HML@CMCS/PVA. Therefore, the physical properties of the material, such as its mechanical properties, can be improved via interactions between different molecules.

3.7. In Vitro Antifungal Properties

As shown in Figure 6, the growth of *F. oxysporum* at 3, 5, and 7 d was observed in order to assess the antifungal activity of CMCS/PVA and HML@CMCS/PVA. At 3 d, no significant difference was observed in the normal growth of mycelium in the control and CMCS/PVA-treated groups, whereas mycelium in the HML@CMCS/PVA-treated group had shown significant inhibitory activity. At 5 d, the mycelium of the control and CMCS/PVA-treated groups still grew normally, while a large antifungal zone appeared around the HML@CMCS/PVA-treated group, which indicated excellent inhibitory activity against the growth of *F. oxysporum*. At 7 d, the mycelial growth of the control and CMCS/PVA groups exceeded 9 cm, in contrast to the HML@CMCS/PVA treatment, which showed significantly slower mycelial growth with the formation of an inhibitory ring around the film. Thus, the prepared HML@CMCS/PVA was effective in preventing the farmland threat of SRR by inhibiting the growth of *F. oxysporum*.

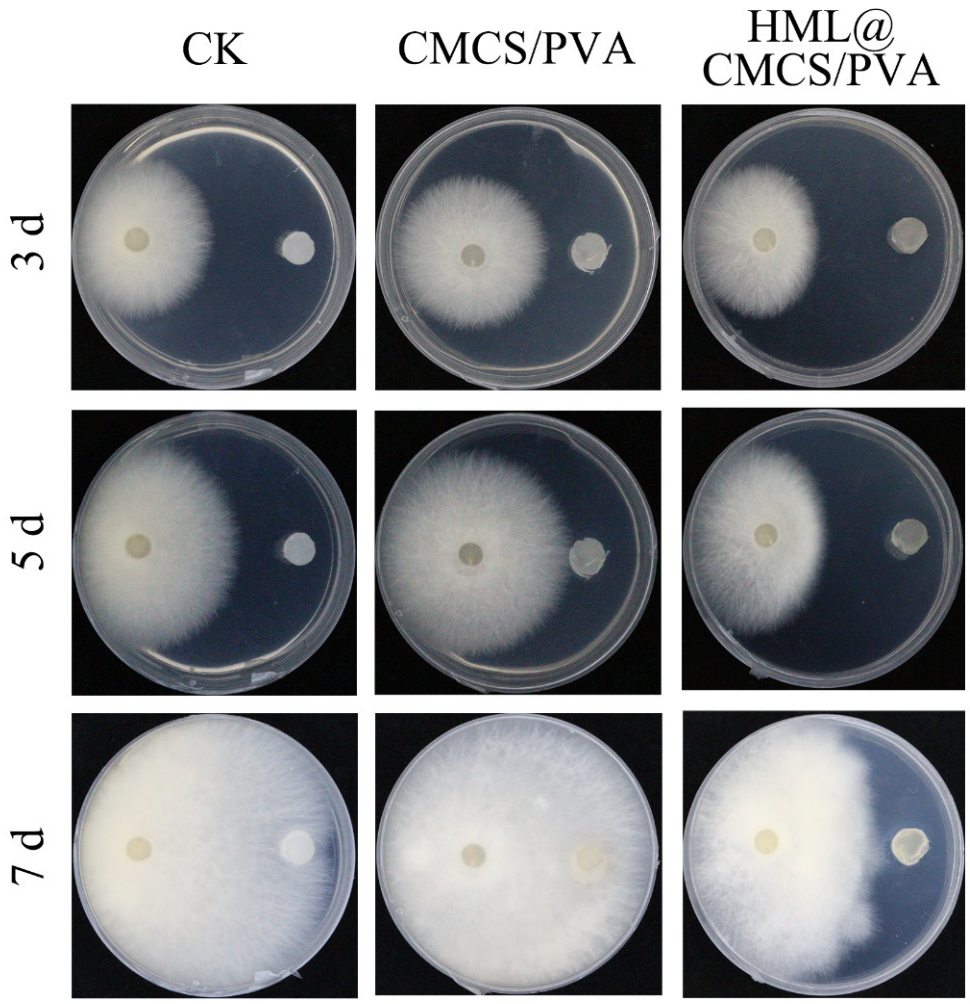

Figure 6. The antifungal activity of sterilized filter paper, CMCS/PVA, and HML@CMCS/PVA against *F. oxysporum* cultured for 3, 5, and 7 d.

3.8. Soil Degradation Experiments

The degradation of the films in soil over a period of 7 d along with the rate of degradation is shown in Figure 7A, B. As can be seen from the figures, all the composite films showed varying degrees of weight loss, indicating that the composite films are biodegradable in a soil environment. Meanwhile, the gradual decomposition and degradation of HML@CMCS/PVA was evident over time, while the appearance and morphology of the commercial membranes remained unchanged. After 7 d, HML@CMCS/PVA degraded up to 58%, while the degradation of the commercial membranes remained unchanged at 0%. The reason for this phenomenon is that in the presence of soil microorganisms and water, the chemical bonds between the biodegradable film and the degraded polymer are readily broken, and the lack of natural conditions in the soil that allow for the degradation of plastic films leads to a long degradation process [57–59].

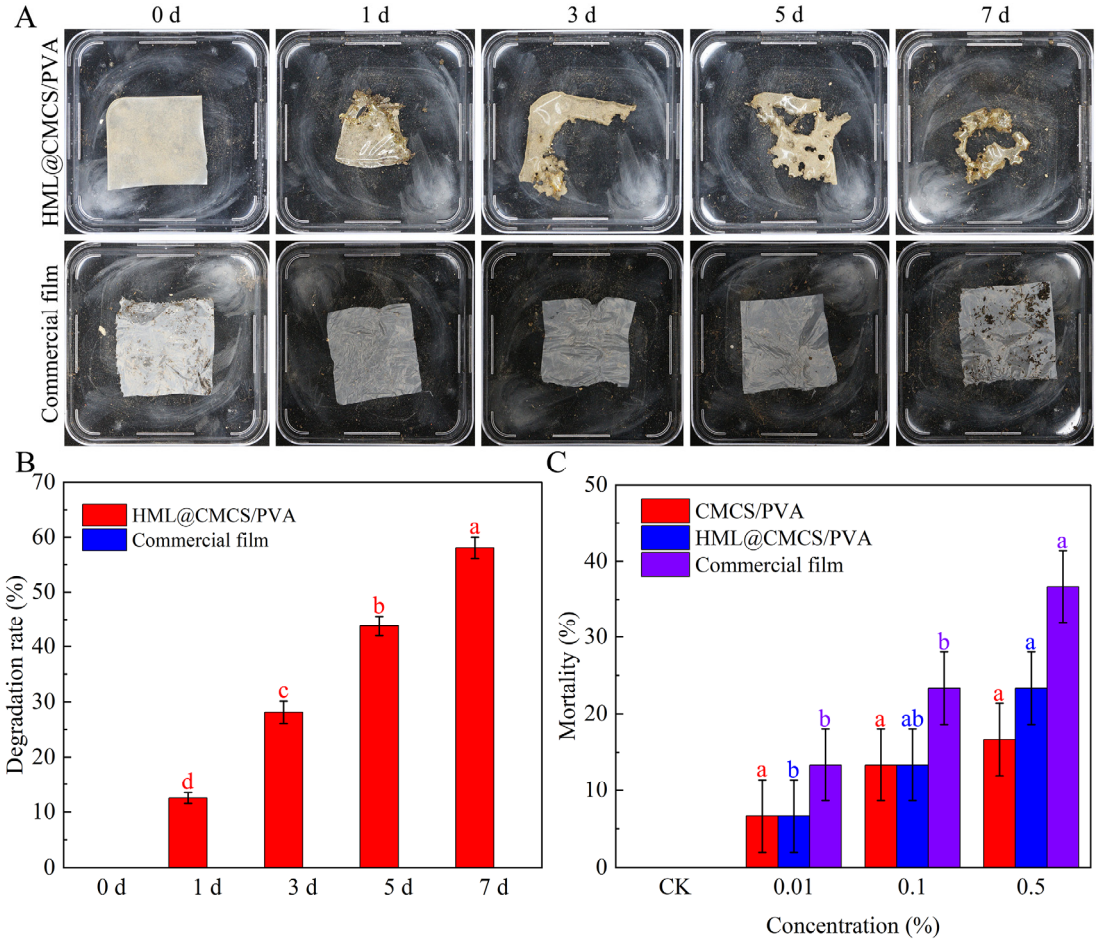

Figure 7. Soil degradation images within 7 d (**A**), degradation rate (**B**), and toxicity to earthworms (**C**) of different film samples. Different letters for the same test parameter indicate significant differences among different groups ($p < 0.05$).

3.9. Biosafety of Films to Earthworms

After the starvation of earthworms for 1 d [28], the mortality of earthworms relative to the microplastics produced by different film materials over a period of 7 d is shown in Figure 7C. The effect of microplastics on earthworms was weak at low concentrations (<0.5%), and the adverse effect of microplastics on earthworms increased significantly when earthworms were exposed to high concentrations (≥0.5%). This observation is consistent with other reports [60]. At the same concentration, the highest earthworm mortality was observed in the commercial film treatment, while the lowest mortality was observed in the CMCS/PVA treatment. At 0.5% concentration, earthworm mortality was 36.67, 16.67, and 23.33% in the commercial film, CMCS/PVA, and HML@CMCS/PVA treatments, respectively. Furthermore, the mortality rate increased with increasing microplastic concentrations in the soil. This is due to the metabolic effects of natural polymer films metabolized in the gut after ingestion by earthworms; the difficult-to-metabolize commercial films produce microplastics that accumulate in large quantities in the gut of earthworms, disrupting their immune systems, which in turn affects the feeding behavior and growth of earthworms. HML in films can also have a negative effect on earthworms, but this effect is very weak compared to commercial films [61]. Therefore, replacing commercial films with HML@CMCS/PVA is an effective measure to reduce the threat of microplastics to earthworms in the soil.

4. Conclusions

In this study, biodegradable films loaded with hymexazol were prepared by blending the polymer carboxymethyl chitosan with polyvinyl alcohol. The results obtained are as follows. The microstructure of the film was observed, and the smooth and uniform surface and dense cryofractured surface showed that there was good cross-linking between different polymer molecules. The tensile strength and elongation at break reached 13.7 MPa and 124.7%, respectively, and the water content, water solubility and water vapor transmission rates were 35%, 28%, and 0.7716 g mm/h m^2 kPa, respectively. The opacity at 600 nm was only 1.92. In addition, the films produced showed excellent antifungal activity against *Fusarium oxysporum*. Finally, the degradation rates of the film were 58% within 7 d, proving the excellent degradation properties of the film. The mortality rate of earthworms (23.33%) was significantly lower than that of the commercial films (36.67%), which indicates excellent soil biosafety. This study confirms that the film prepared by blending CMCS with PVA has excellent mechanical properties and barrier properties, which provide a new way to prevent soybean root rot and reduce the pollution of agricultural films.

Author Contributions: Conceptualization, Z.L. and J.F.; methodology, Z.L. and X.M.; software, S.S. and T.J.; validation, S.Z. and J.F.; formal analysis, Z.L. and T.J.; investigation, Z.L. and X.M.; resources, J.F.; data curation, Z.L., S.S. and S.Z.; writing—original draft preparation, Z.L.; writing—review and editing, Z.L. and J.F.; visualization, J.F.; supervision, J.F.; project administration, J.F.; funding acquisition, J.F. All authors have read and agreed to the published version of the manuscript.

Funding: This research was funded by Jiangsu Province Carbon Peaking Carbon Neutrality Science and Technology Innovation Special Fund Project (BE2022425).

Data Availability Statement: No data was used for the research described in the article.

Acknowledgments: The authors thank all the editors and reviewers for their comments on this manuscript.

Conflicts of Interest: The authors declare that they have no known competing financial interest or personal relationships that could have appeared to influence the work reported in this paper.

References

1. Chang, X.; Wei, D.; Zeng, Y.; Zhao, X.; Hu, Y.; Wu, X.; Song, C.; Gong, G.; Chen, H.; Yang, C.; et al. Maize-soybean relay strip intercropping reshapes the rhizosphere bacterial community and recruits beneficial bacteria to suppress Fusarium root rot of soybean. *Front. Microbiol.* **2022**, *13*, 1009689. [CrossRef] [PubMed]
2. Naeem, M.; Munir, M.; Li, H.; Raza, M.A.; Song, C.; Wu, X.; Irshad, G.; Khalid, M.H.B.; Yang, W.; Chang, X. Transcriptional Responses of *Fusarium graminearum* Interacted with Soybean to Cause Root Rot. *J. Fungi* **2021**, *7*, 422. [CrossRef] [PubMed]
3. Barros, G.G.; Zanon, M.S.A.; Chiotta, M.L.; Reynoso, M.M.; Scandiani, M.M.; Chulze, S.N. Pathogenicity of phylogenetic species in the Fusarium graminearum complex on soybean seedlings in Argentina. *Eur. J. Plant Pathol.* **2013**, *138*, 215–222. [CrossRef]
4. Xu, H.; Yan, L.; Zhang, M.; Chang, X.; Zhu, D.; Wei, D.; Naeem, M.; Song, C.; Wu, X.; Liu, T.; et al. Changes in the Density and Composition of Rhizosphere Pathogenic Fusarium and Beneficial Trichoderma Contributing to Reduced Root Rot of Intercropped Soybean. *Pathogens* **2022**, *11*, 478. [CrossRef] [PubMed]
5. Cruz, D.R.; Leandro, L.F.S.; Mayfield, D.A.; Meng, Y.; Munkvold, G.P. Effects of Soil Conditions on Root Rot of Soybean Caused by *Fusarium graminearum*. *Phytopathology* **2020**, *110*, 1693–1703. [CrossRef] [PubMed]
6. Zhang, W.; Li, S.; Shen, Y.; Yue, S. Film mulching affects root growth and function in dryland maize-soybean intercropping. *Field Crops Res.* **2021**, *271*, 108240. [CrossRef]
7. Zhang, X.-L.; Zhao, Y.-Y.; Zhang, X.-T.; Shi, X.-P.; Shi, X.-Y.; Li, F.-M. Re-used mulching of plastic film is more profitable and environmentally friendly than new mulching. *Soil Tillage Res.* **2022**, *216*, 105256. [CrossRef]
8. Helmberger, M.S.; Tiemann, L.K.; Grieshop, M.J.; Morriën, E. Towards an ecology of soil microplastics. *Funct. Ecol.* **2019**, *34*, 550–560. [CrossRef]
9. Kedzierski, M.; Cirederf-Boulant, D.; Palazot, M.; Yvin, M.; Bruzaud, S. Continents of plastics: An estimate of the stock of microplastics in agricultural soils. *Sci. Total Environ.* **2023**, *880*, 163294. [CrossRef]
10. Panda, P.K.; Sadeghi, K.; Seo, J. Recent advances in poly (vinyl alcohol)/natural polymer based films for food packaging applications: A review. *Food Packag. Shelf Life* **2022**, *33*, 100904. [CrossRef]
11. El Hadrami, A.; Adam, L.R.; El Hadrami, I.; Daayf, F. Chitosan in plant protection. *Mar. Drugs* **2010**, *8*, 968–987. [CrossRef]
12. Razmjoo, F.; Sadeghi, E.; Rouhi, M.; Mohammadi, R.; Noroozi, R.; Safajoo, S. Polyvinyl alcohol—Zedo gum edible film: Physical, mechanical and thermal properties. *J. Appl. Polym. Sci.* **2020**, *138*, 49875. [CrossRef]

13. Xie, B.; Zhang, X.; Luo, X.; Wang, Y.; Li, Y.; Li, B.; Liu, S. Edible coating based on beeswax-in-water Pickering emulsion stabilized by cellulose nanofibrils and carboxymethyl chitosan. *Food Chem.* **2020**, *331*, 127108. [CrossRef]
14. Kritchenkov, A.S.; Egorov, A.R.; Volkova, O.V.; Artemjev, A.A.; Kurliuk, A.V.; Anh Le, T.; Hieu Truong, H.; Le-Nhat-Thuy, G.; Van Tran Thi, T.; Van Tuyen, N.; et al. Novel biopolymer-based nanocomposite food coatings that exhibit active and smart properties due to a single type of nanoparticles. *Food Chem.* **2021**, *343*, 128676. [CrossRef]
15. Kritchenkov, A.S.; Egorov, A.R.; Volkova, O.V.; Zabodalova, L.A.; Suchkova, E.P.; Yagafarov, N.Z.; Kurasova, M.N.; Dysin, A.P.; Kurliuk, A.V.; Shakola, T.V.; et al. Active antibacterial food coatings based on blends of succinyl chitosan and triazole betaine chitosan derivatives. *Food Packag. Shelf Life* **2020**, *25*, 100534. [CrossRef]
16. Zimet, P.; Mombru, A.W.; Mombru, D.; Castro, A.; Villanueva, J.P.; Pardo, H.; Rufo, C. Physico-chemical and antilisterial properties of nisin-incorporated chitosan/carboxymethyl chitosan films. *Carbohydr. Polym.* **2019**, *219*, 334–343. [CrossRef]
17. de Lacerda Bukzem, A.; Dos Santos, D.M.; Leite, I.S.; Inada, N.M.; Campana-Filho, S.P. Tuning the properties of carboxymethylchitosan-based porous membranes for potential application as wound dressing. *Int. J. Biol. Macromol.* **2021**, *166*, 459–470. [CrossRef]
18. Wang, Y.; Cen, C.; Chen, J.; Fu, L. MgO/carboxymethyl chitosan nanocomposite improves thermal stability, waterproof and antibacterial performance for food packaging. *Carbohydr. Polym.* **2020**, *236*, 116078. [CrossRef]
19. Mitrea, L.; Calinoiu, L.F.; Martau, G.A.; Szabo, K.; Teleky, B.E.; Muresan, V.; Rusu, A.V.; Socol, C.T.; Vodnar, D.C. Poly(vinyl alcohol)-Based Biofilms Plasticized with Polyols and Colored with Pigments Extracted from Tomato By-Products. *Polymers* **2020**, *12*, 532. [CrossRef]
20. Panda, P.K.; Park, K.; Seo, J. Development of poly (vinyl alcohol)/regenerated chitosan blend film with superior barrier, antioxidant, and antibacterial properties. *Prog. Org. Coat.* **2023**, *183*, 107749. [CrossRef]
21. Kanatt, S.R.; Rao, M.S.; Chawla, S.P.; Sharma, A. Active chitosan–polyvinyl alcohol films with natural extracts. *Food Hydrocoll.* **2012**, *29*, 290–297. [CrossRef]
22. Yang, W.; Owczarek, J.S.; Fortunati, E.; Kozanecki, M.; Mazzaglia, A.; Balestra, G.M.; Kenny, J.M.; Torre, L.; Puglia, D. Antioxidant and antibacterial lignin nanoparticles in polyvinyl alcohol/chitosan films for active packaging. *Ind. Crops Prod.* **2016**, *94*, 800–811. [CrossRef]
23. Liang, W.; Zhao, Y.; Xiao, D.; Cheng, J.; Zhao, J. A biodegradable water-triggered chitosan/hydroxypropyl methylcellulose pesticide mulch film for sustained control of Phytophthora sojae in soybean (*Glycine max* L. Merr.). *J. Clean. Prod.* **2020**, *245*, 118943. [CrossRef]
24. Bonilla, J.; Fortunati, E.; Vargas, M.; Chiralt, A.; Kenny, J.M. Effects of chitosan on the physicochemical and antimicrobial properties of PLA films. *J. Food Eng.* **2013**, *119*, 236–243. [CrossRef]
25. Ekambaram, K.; Doraisamy, M. Fouling resistant PVDF/Carboxymethyl chitosan composite nanofiltration membranes for humic acid removal. *Carbohydr. Polym.* **2017**, *173*, 431–440. [CrossRef]
26. Pereira, V.A.; de Arruda, I.N.Q.; Stefani, R. Active chitosan/PVA films with anthocyanins from Brassica oleraceae (Red Cabbage) as Time–Temperature Indicators for application in intelligent food packaging. *Food Hydrocoll.* **2015**, *43*, 180–188. [CrossRef]
27. Atarés, L.; Bonilla, J.; Chiralt, A. Characterization of sodium caseinate-based edible films incorporated with cinnamon or ginger essential oils. *J. Food Eng.* **2010**, *100*, 678–687. [CrossRef]
28. Ding, W.; Li, Z.; Qi, R.; Jones, D.L.; Liu, Q.; Liu, Q.; Yan, C. Effect thresholds for the earthworm Eisenia fetida: Toxicity comparison between conventional and biodegradable microplastics. *Sci. Total Environ.* **2021**, *781*, 146884. [CrossRef]
29. La Mantia, F.P.; Ascione, L.; Mistretta, M.C.; Rapisarda, M.; Rizzarelli, P. Comparative Investigation on the Soil Burial Degradation Behaviour of Polymer Films for Agriculture before and after Photo-Oxidation. *Polymers* **2020**, *12*, 753. [CrossRef]
30. Zhang, Y.; Zhao, W.; Lin, Z.; Tang, Z.; Lin, B. Carboxymethyl chitosan/sodium alginate hydrogel films with good biocompatibility and reproducibility by in situ ultra-fast crosslinking for efficient preservation of strawberry. *Carbohydr. Polym.* **2023**, *316*, 121073. [CrossRef]
31. Tao, F.; Cheng, Y.; Tao, H.; Jin, L.; Wan, Z.; Dai, F.; Xiang, W.; Deng, H. Carboxymethyl chitosan/sodium alginate-based micron-fibers fabricated by emulsion electrospinning for periosteal tissue engineering. *Mater. Des.* **2020**, *194*, 108849. [CrossRef]
32. Yang, H.; Guo, X.; Chen, R.; Liu, Q.; Liu, J.; Yu, J.; Lin, C.; Wang, J.; Zhang, M. Enhanced anti-biofouling ability of polyurethane anti-cavitation coating with ZIF-8: A comparative study of various sizes of ZIF-8 on coating. *Eur. Polym. J.* **2021**, *144*, 110212. [CrossRef]
33. Samide, A.; Iacobescu, G.E.; Tutunaru, B.; Iordache, S. Silver nanoparticles/polyvinyl alcohol film: Studies of thermal characterization, AFM and corrosion protection by electrodeposition on 304L stainless steel. *J. Therm. Anal. Calorim.* **2021**, *147*, 1041–1051. [CrossRef]
34. Yin, M.; Chen, X.; Li, R.; Huang, D.; Fan, X.; Ren, X.; Huang, T.-S. Preparation and characterization of antimicrobial PVA hybrid films withN-halamine modified chitosan nanospheres. *J. Appl. Polym. Sci.* **2016**, *133*, 44204. [CrossRef]
35. Yoon, S.D.; Kim, Y.M.; Kim, B.I.; Je, J.Y. Preparation and antibacterial activities of chitosan-gallic acid/polyvinyl alcohol blend film by LED-UV irradiation. *J. Photochem. Photobiol. B* **2017**, *176*, 145–149. [CrossRef]
36. Yin, M.; Lin, X.; Ren, T.; Li, Z.; Ren, X.; Huang, T.S. Cytocompatible quaternized carboxymethyl chitosan/poly(vinyl alcohol) blend film loaded copper for antibacterial application. *Int. J. Biol. Macromol.* **2018**, *120*, 992–998. [CrossRef]
37. Sun, W.; Liu, X.; Li, X.; Wang, S.; Li, Q.; Sun, Z. A method for the treatment of black tea waste: Converting it into liquid mulching film and solid mulching film. *J. Appl. Polym. Sci.* **2022**, *140*, e53481. [CrossRef]

38. Wang, L.-C.; Chen, X.-G.; Yu, L.-J.; Li, P.-W. Controlled drug release through carboxymethyl-chitosan/poly(vinyl alcohol) blend films. *Polym. Eng. Sci.* **2007**, *47*, 1373–1379. [CrossRef]
39. Meera, K.; Ramesan, M.T. Performance of Boehmite Nanoparticles Reinforced Carboxymethyl Chitosan/Polyvinyl Alcohol Blend Nanocomposites Tailored Through Green Synthesis. *J. Polym. Environ.* **2022**, *31*, 447–460. [CrossRef]
40. Yang, N.; Sun, Z.-X.; Feng, L.-S.; Zheng, M.-Z.; Chi, D.-C.; Meng, W.-Z.; Hou, Z.-Y.; Bai, W.; Li, K.-Y. Plastic Film Mulching for Water-Efficient Agricultural Applications and Degradable Films Materials Development Research. *Mater. Manuf. Process.* **2014**, *30*, 143–154. [CrossRef]
41. Adhikari, R.; Bristow, K.L.; Casey, P.S.; Freischmidt, G.; Hornbuckle, J.W.; Adhikari, B. Preformed and sprayable polymeric mulch film to improve agricultural water use efficiency. *Agric. Water Manag.* **2016**, *169*, 1–13. [CrossRef]
42. Zhang, X.; Gao, D.; Luo, W.; Xiao, N.; Xiao, G.; Li, Z.; Liu, C. Hemicelluloses-based sprayable and biodegradable pesticide mulch films for Chinese cabbage growth. *Int. J. Biol. Macromol.* **2023**, *225*, 1350–1360. [CrossRef] [PubMed]
43. Xie, Z.; Xiong, Q.; Fang, Y.; Zhang, Q.; Liang, W.; Cheng, J.; Shang, W.; Zhao, W.; Zhao, J. Novel Biodegradable Composite Mulch Film Embedded with Temperature-Responsive Pesticide Microcapsules for Durable Control of Phytophthora Root Rot on Soybean. *ACS Sustain. Chem. Eng.* **2023**, *11*, 9868–9879. [CrossRef]
44. Briassoulis, D.; Giannoulis, A. Evaluation of the functionality of bio-based plastic mulching films. *Polym. Test.* **2018**, *67*, 99–109. [CrossRef]
45. Suriyatem, R.; Auras, R.A.; Rachtanapun, P. Improvement of mechanical properties and thermal stability of biodegradable rice starch–based films blended with carboxymethyl chitosan. *Ind. Crops Prod.* **2018**, *122*, 37–48. [CrossRef]
46. Wu, J.; Zhong, F.; Li, Y.; Shoemaker, C.F.; Xia, W. Preparation and characterization of pullulan–chitosan and pullulan–carboxymethyl chitosan blended films. *Food Hydrocoll.* **2013**, *30*, 82–91. [CrossRef]
47. Lan, W.; He, L.; Liu, Y. Preparation and Properties of Sodium Carboxymethyl Cellulose/Sodium Alginate/Chitosan Composite Film. *Coatings* **2018**, *8*, 291. [CrossRef]
48. Zhuang, T.T.; Liu, Y.; Li, Y.; Zhao, Y.; Wu, L.; Jiang, J.; Yu, S.H. Integration of Semiconducting Sulfides for Full-Spectrum Solar Energy Absorption and Efficient Charge Separation. *Angew. Chem. Int. Ed. Engl.* **2016**, *55*, 6396–6400. [CrossRef]
49. Cui, J.; Li, Y.; Liu, L.; Chen, L.; Xu, J.; Ma, J.; Fang, G.; Zhu, E.; Wu, H.; Zhao, L.; et al. Near-Infrared Plasmonic-Enhanced Solar Energy Harvest for Highly Efficient Photocatalytic Reactions. *Nano Lett.* **2015**, *15*, 6295–6301. [CrossRef]
50. Zhao, J.; Jiang, H.; Huang, Q.; Xu, J.; Duan, M.; Yu, S.; Zhi, Z.; Pang, J.; Wu, C. Carboxymethyl chitosan incorporated with gliadin/phlorotannin nanoparticles enables the formation of new active packaging films. *Int. J. Biol. Macromol.* **2022**, *203*, 40–48. [CrossRef]
51. Wang, L.; Lei, L.; Wan, K.; Fu, Y.; Hu, H. Physicochemical Properties and Biological Activity of Active Films Based on Corn Peptide Incorporated Carboxymethyl Chitosan. *Coatings* **2021**, *11*, 604. [CrossRef]
52. Hong, J.; Chen, R.; Zeng, X.A.; Han, Z. Effect of pulsed electric fields assisted acetylation on morphological, structural and functional characteristics of potato starch. *Food Chem.* **2016**, *192*, 15–24. [CrossRef] [PubMed]
53. Liu, L.; Liu, Y.; Liu, Y.; Wang, Q. Efficient flame retardant polyvinyl alcohol membrane through surface graft method. *RSC Adv.* **2016**, *6*, 35051–35057. [CrossRef]
54. Zhao, M.; Zhou, H.; Chen, L.; Hao, L.; Chen, H.; Zhou, X. Carboxymethyl chitosan grafted trisiloxane surfactant nanoparticles with pH sensitivity for sustained release of pesticide. *Carbohydr. Polym.* **2020**, *243*, 116433. [CrossRef] [PubMed]
55. Rao, K.M.; Sudhakar, K.; Suneetha, M.; Won, S.Y.; Han, S.S. Fungal-derived carboxymethyl chitosan blended with polyvinyl alcohol as membranes for wound dressings. *Int. J. Biol. Macromol.* **2021**, *190*, 792–800. [CrossRef] [PubMed]
56. Choo, K.; Ching, Y.C.; Chuah, C.H.; Julai, S.; Liou, N.S. Preparation and Characterization of Polyvinyl Alcohol-Chitosan Composite Films Reinforced with Cellulose Nanofiber. *Materials* **2016**, *9*, 644. [CrossRef]
57. Liu, J.; Zhu, L.; Luo, S.; Bu, L.; Chen, X.; Yue, S.; Li, S. Response of nitrous oxide emission to soil mulching and nitrogen fertilization in semi-arid farmland. *Agric. Ecosyst. Environ.* **2014**, *188*, 20–28. [CrossRef]
58. Pires, J.R.A.; Souza, V.G.L.; Fucinos, P.; Pastrana, L.; Fernando, A.L. Methodologies to Assess the Biodegradability of Bio-Based Polymers-Current Knowledge and Existing Gaps. *Polymers* **2022**, *14*, 1359. [CrossRef]
59. Gao, X.; Xie, D.; Yang, C. Effects of a PLA/PBAT biodegradable film mulch as a replacement of polyethylene film and their residues on crop and soil environment. *Agric. Water Manag.* **2021**, *255*, 107053. [CrossRef]
60. Zhang, L.; Sintim, H.Y.; Bary, A.I.; Hayes, D.G.; Wadsworth, L.C.; Anunciado, M.B.; Flury, M. Interaction of *Lumbricus terrestris* with macroscopic polyethylene and biodegradable plastic mulch. *Sci. Total Environ.* **2018**, *635*, 1600–1608. [CrossRef]
61. Food SecurityCheng, Y.; Zhu, L.; Song, W.; Jiang, C.; Li, B.; Du, Z.; Wang, J.; Wang, J.; Li, D.; Zhang, K. Combined effects of mulch film-derived microplastics and atrazine on oxidative stress and gene expression in earthworm (*Eisenia fetida*). *Sci. Total Environ.* **2020**, *746*, 141280. [CrossRef]